Mercury Isotopes in Earth and Environmental Sciences

Joel D. Blum, Laura S. Sherman, and Marcus W. Johnson

Department of Earth and Environmental Sciences, University of Michigan, Ann Arbor, Michigan 48109; email: jdblum@umich.edu, lsaylors@umich.edu, mwj@umich.edu

Annu. Rev. Earth Planet. Sci. 2014. 42:249–69

First published online as a Review in Advance on February 21, 2014

The *Annual Review of Earth and Planetary Sciences* is online at earth.annualreviews.org

This article's doi: 10.1146/annurev-earth-050212-124107

Keywords

mass-dependent fractionation, mass-independent fractionation, biogeochemistry, heavy metals

Abstract

Virtually all biotic, dark abiotic, and photochemical transformations of mercury (Hg) produce Hg isotope fractionation, which can be either mass dependent (MDF) or mass independent (MIF). The largest range in MDF is observed among geological materials and rainfall impacted by anthropogenic sources. The largest positive MIF of Hg isotopes (odd-mass excess) is caused by photochemical degradation of methylmercury in water. This signature is retained through the food web and measured in all freshwater and marine fish. The largest negative MIF of Hg isotopes (odd-mass deficit) is caused by photochemical reduction of inorganic Hg and has been observed in Arctic snow and plant foliage. Ratios of MDF to MIF and ratios of ^{199}Hg MIF to ^{201}Hg MIF are often diagnostic of biogeochemical reaction pathways. More than a decade of research demonstrates that Hg isotopes can be used to trace sources, biogeochemical cycling, and reactions involving Hg in the environment.

INTRODUCTION

The study of natural variability in the isotopic composition of mercury (Hg) in Earth and environmental materials using modern mass spectrometry methods began over a decade ago (Jackson 2001, Lauretta et al. 2001). This area of research has grown rapidly, stimulated by improvements in measurement precision (Foucher & Hintelmann 2006, Smith et al. 2005) and the demonstration that mass-independent fractionation (MIF) of Hg isotopes is common in the environment (Bergquist & Blum 2007). More than 100 papers focused on natural variations in Hg isotope ratios have now been published, making it impractical to conduct an all-inclusive review of the literature. Intense interest in Hg isotopes stems from the facts that Hg can become a potent neurotoxin in the environment and that Hg isotopes can be used to trace environmental exposure to this pollutant. In addition, the different redox states of Hg have highly contrasting chemical behaviors, and fractionation of Hg isotopes provides a tracer of many redox-sensitive processes (Blum 2011). Of particular importance is the observation that Hg undergoes several types of isotope fractionation that follow fundamentally different chemical mechanisms (Bergquist & Blum 2009). These include both biotic and abiotic mass-dependent fractionation (MDF), MIF caused by the magnetic isotope effect (Bergquist & Blum 2007), and MIF caused by the nuclear volume effect (Estrade et al. 2009). In addition, one study has suggested that a wavelength-dependent MIF effect may occur during photochemical oxidation of Hg in the upper atmosphere (Chen et al. 2012), perhaps by a process similar to that observed in Hg vapor lamps (Mead et al. 2013).

Several reviews of Hg isotopes have preceded this contribution. Ridley & Stetson (2006) reviewed some of the early papers on Hg isotopes. Bergquist & Blum (2009) provided an overview of fractionation in natural and experimental systems. Yin et al. (2010) reviewed some key studies of Hg isotopes in environmental systems, and Blum (2011) provided a comprehensive summary of papers published up to that time on experimental Hg isotope fractionation and Hg isotope variation in the environment. Finally, Hintelmann (2012) provided a general review with emphasis on issues involved in Hg isotope measurements and experimental fractionation studies. This article does not repeat the contributions of previous reviews, nor does it attempt to summarize the conclusions of the numerous papers published on Hg isotopes. Instead, it concentrates on studies of Hg isotope variations in geological and environmental samples and combines data from more than 50 published studies to explore the overarching trends in natural Hg isotopic variation. We use this compilation to characterize the Hg isotopic composition of various Earth reservoirs and to better understand the biogeochemical processes that lead to large-magnitude Hg isotopic variability.

MERCURY SPECIATION AND THE MERCURY CYCLE

It has been estimated that present-day anthropogenic emissions of Hg are approximately three times greater than natural emissions (Mason et al. 1994). Primary anthropogenic emissions are dominated by coal combustion, cement production, and waste incineration, whereas natural emissions are largely related to volcanic and hydrothermal systems (US EPA 1997). There is also a growing reservoir of previously deposited anthropogenic Hg that can be re-emitted from aquatic and terrestrial reservoirs (Gustin et al. 2008).

The chemical speciation of Hg dramatically affects its mobility and toxicity. Hg can exist in a number of phases including stable solids (e.g., HgS minerals and Hg-S complexes in sediments), a highly bioaccumulative methylated form (methylmercury, MeHg), and gaseous and aerosol phases in the atmosphere (Morel et al. 1998, Schroeder & Munthe 1998). Details of atmospheric Hg speciation are not well understood, but three operationally defined forms are generally measured:

gaseous elemental Hg [Hg(0)], reactive gaseous Hg (RGM), and fine particle–bound Hg (Hg_p). Hg(0) has a relatively long atmospheric residence time (~1 year), but once it is oxidized it becomes reactive and is rapidly deposited in wet and dry deposition (Schroeder & Munthe 1998). As a result of this atmospheric cycling, Hg is distributed and deposited globally (Douglas et al. 2008, Lindberg et al. 2002).

In aqueous solutions, Hg can exist as a dissolved gas, as an oxidized ligand-bound species, or as dissolved MeHg. Both microbial and photochemical reactions can cause the reduction of ligand-bound Hg(II) and MeHg in solution to produce Hg(0) (Fitzgerald & Lamborg 2003). In addition, some sulfate- and iron-reducing bacteria can methylate Hg(II) to MeHg. Once it is produced, MeHg can be bioaccumulated in aquatic and terrestrial food webs, reaching potentially hazardous levels in piscivorous fish, insectivorous birds, and mammals (Evers et al. 2007). In most countries, the primary pathway for human exposure to MeHg is the consumption of marine and freshwater fish (Sunderland 2007).

MERCURY ISOTOPE RATIO NOMENCLATURE

Hg has seven stable isotopes with the following abundances in the National Institute of Standards and Technology (NIST) Standard Reference Material (SRM) 3133: $^{196}Hg = 0.16\%$, $^{198}Hg = 10.04\%$, $^{199}Hg = 16.94\%$, $^{200}Hg = 23.14\%$, $^{201}Hg = 13.17\%$, $^{202}Hg = 29.73\%$, and $^{204}Hg = 6.83\%$, as referenced to the certified $^{205}Tl/^{203}Tl$ ratio of 2.38714 (Blum & Bergquist 2007). Hg isotopic compositions are reported as

$$\delta^{xxx}Hg(‰) = ([(^{xxx}Hg/^{198}Hg)_{unknown}/(^{xxx}Hg/^{198}Hg)_{SRM3133}] - 1) \times 1000.$$

The use of ^{198}Hg as the denominator in $\delta^{xxx}Hg$ values has been adopted by most research groups and has been highly recommended (Blum & Bergquist 2007). The convention in stable isotope geochemistry is to report isotope fractionation using ratios with the smaller mass in the denominator so that higher delta values always signify a heavier average isotopic mass. In fact, delta values are defined in this manner for all of the more than 25 elements for which stable isotopic compositions are commonly studied (Coplen 2011, Johnson et al. 2004, Porcelli & Baskaran 2011). The first papers reporting high-precision Hg isotope ratios adopted the $^{202}Hg/^{198}Hg$ ratio for expressing MDF (Foucher & Hintelmann 2006, Smith et al. 2005) because ^{198}Hg is the lowest mass isotope of sufficient abundance for accurate measurement and ^{202}Hg is the highest mass isotope free of isobaric interferences (i.e., ^{204}Pb). To avoid the confusion of using several different reference isotope ratios, a problem that plagued several other stable isotope systems at their outset, Blum & Bergquist (2007) urged the then-fledgling Hg isotope community to adopt the $^{202}Hg/^{198}Hg$ ratio and NIST SRM 3133 in the definition of $\delta^{202}Hg$ and to use this as a measure of MDF. Of the 15 research groups that have published Hg isotope ratio measurements, 13 follow this convention. Consequently, in the vast majority (>95%) of published papers on Hg isotopes, $\delta^{202}Hg$ is defined using the $^{202}Hg/^{198}Hg$ ratio referenced to NIST SRM 3133, facilitating direct comparison of results. The two exceptions are a research group at Environment Canada who used ^{202}Hg as the denominator isotope for Hg isotope ratios and a non-NIST-traceable Hg standard solution for sample-standard bracketing (Jackson & Muir 2012; Jackson et al. 2004, 2008, 2013) and a research group at Florida State University who used ^{200}Hg as the denominator isotope (Das et al. 2009, Ghosh et al. 2008).

In addition to MDF, many researchers have observed significant MIF of the odd-mass-number isotopes of Hg, and several recent studies suggest that the even-mass-number isotopes of Hg can also undergo MIF. MIF is measured as the difference between a measured δ-value and that predicted on the basis of the measured $\delta^{202}Hg$ value and the kinetic MDF law derived from

transition state theory. For variations of less than ~10‰, these values are approximated as (Blum & Bergquist 2007)

$$\Delta^{199}\mathrm{Hg} = \delta^{199}\mathrm{Hg} - (\delta^{202}\mathrm{Hg} \times 0.2520)$$

$$\Delta^{200}\mathrm{Hg} = \delta^{200}\mathrm{Hg} - (\delta^{202}\mathrm{Hg} \times 0.5024)$$

$$\Delta^{201}\mathrm{Hg} = \delta^{201}\mathrm{Hg} - (\delta^{202}\mathrm{Hg} \times 0.7520)$$

$$\Delta^{204}\mathrm{Hg} = \delta^{204}\mathrm{Hg} - (\delta^{202}\mathrm{Hg} \times 1.4930).$$

The odd-mass-number isotopes of Hg undergo the highest degree of MIF due to the magnetic isotope effect, which occurs during photochemical radical pair reactions. Because only the odd-mass-number isotopes have nuclear magnetic moments and nuclear spin, triplet-to-singlet and singlet-to-triplet intersystem crossing is enhanced among these isotopes. This process causes the odd- and even-mass-number isotopes to react at differing rates and often results in high levels of MIF (>1‰). A small amount of MIF (<~0.5‰) can also be produced during equilibrium reactions due to the nuclear volume effect, which occurs because differences in nuclear radii between the isotopes do not scale linearly with mass.

EXPERIMENTAL EVIDENCE OF MERCURY ISOTOPE FRACTIONATION

A wide range of experiments have been carried out with the goal of understanding Hg isotope fractionation during chemical and biological transformations (**Figure 1**). Blum (2011) summarized the experiments published up until the year 2011 to provide a basic framework for understanding MDF and MIF in the environment. Nearly all kinetic reactions involving Hg produce products with lower δ^{202}Hg (i.e., isotopically lighter) and leave a residual pool of reactant with higher δ^{202}Hg (i.e., isotopically heavier). Biotic and dark abiotic reactions do not produce significant MIF (i.e., Δ^{199}Hg does not differ between products and reactants). In contrast, all photochemical reactions that have been studied produce changes in both MDF and MIF. As these reactions proceed, the ratio of Δ^{199}Hg to δ^{202}Hg appears to be diagnostic of the type of reaction. For example, Bergquist & Blum (2007) found that progressive photochemical reduction of Hg(II) from an aqueous solution in the presence of terrestrial organic matter produced Hg(0) and residual Hg(II) that fell along a Δ^{199}Hg/δ^{202}Hg line with a slope of 1.15 ± 0.07 (1 SE), whereas photochemical degradation of MeHg produced Hg(0) and residual MeHg that fell along a Δ^{199}Hg/δ^{202}Hg line with a slope of 2.43 ± 0.10 (1 SE). Sherman et al. (2010) found that in the presence of halogens, photochemical reduction of Hg(II) associated with snow in the Arctic produced product Hg(0) and residual Hg(II) that fell along a Δ^{199}Hg/δ^{202}Hg line with a slope of −3.5 ± 0.32 (1 SE). Finally, Estrade et al. (2009) and Ghosh et al. (2013) found that $\mathrm{Hg(0)_{gas}}$ in equilibrium with $\mathrm{Hg(0)_{liquid}}$ is fractionated to a small extent by the nuclear volume effect and falls on a Δ^{199}Hg/δ^{202}Hg line with a slope of ~0.1.

The ratio of Δ^{199}Hg/Δ^{201}Hg can also be diagnostic of MIF mechanisms and the ligands associated with Hg in aqueous solutions. The experimental studies discussed above have demonstrated that photochemical reduction of $\mathrm{Hg(II)_{aq}}$ to Hg(0) results in a Δ^{199}Hg/Δ^{201}Hg ratio of 1.00 ± 0.01 (1 SE) (Bergquist & Blum 2007), photochemical demethylation of MeHg results in a Δ^{199}Hg/Δ^{201}Hg ratio of 1.34 ± 0.04 (1 SE) (Bergquist & Blum 2007), photochemical reduction of Hg(II) from Arctic snow results in a Δ^{199}Hg/Δ^{201}Hg ratio of 1.07 ± 0.02 (1 SE) (Sherman et al. 2010) and equilibrium evaporation of Hg(0) produces a Δ^{199}Hg/Δ^{201}Hg ratio of 1.59 ± 0.03 (1 SE) (Ghosh et al. 2013).

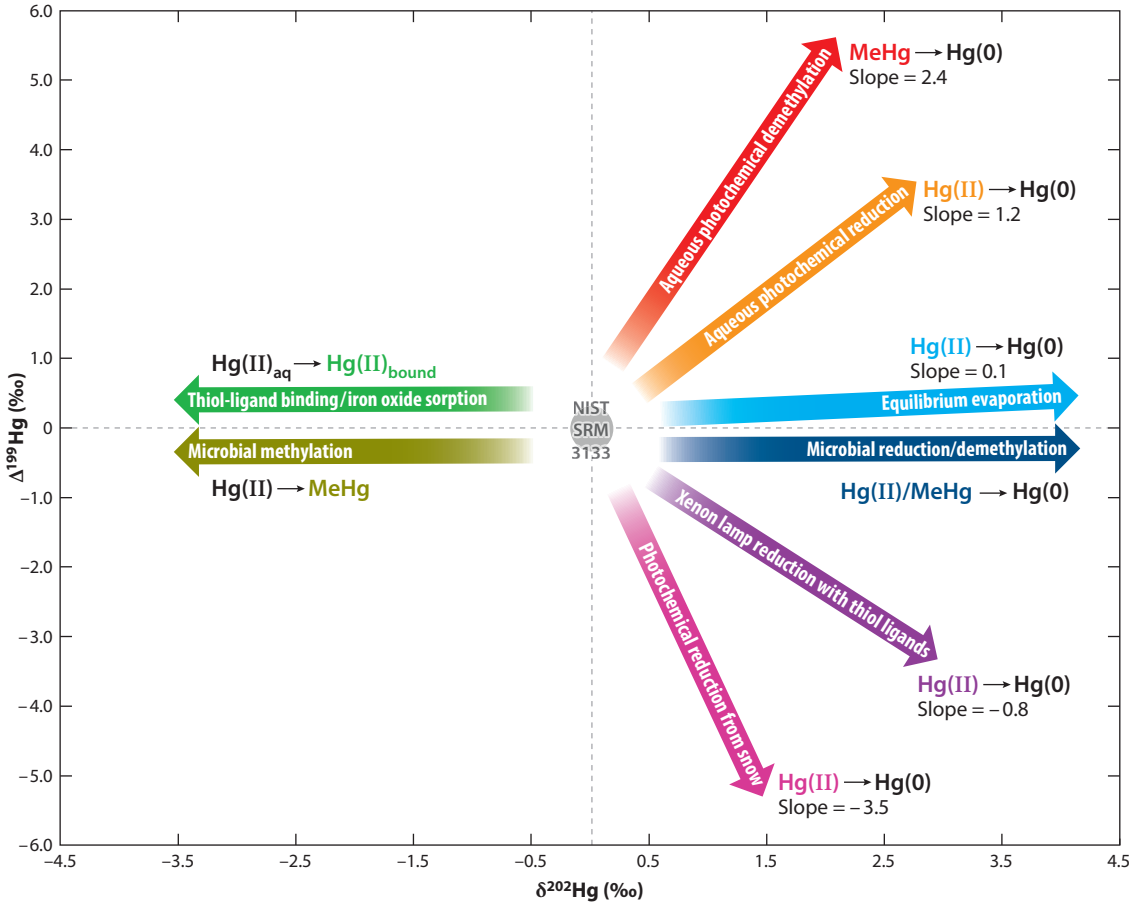

Figure 1

Overview of the general patterns in isotope fractionation that have been observed experimentally (Δ^{199}Hg versus δ^{202}Hg). For comparison, the scale is the same as in **Figure 2**. For each process, the direction of the arrow indicates the isotopic evolution of either the reactant or product as indicated by colored labels. Reactions are as follows: The light blue arrow indicates fractionation during equilibrium evaporation (MIF due to the nuclear volume effect) (Estrade et al. 2009, Ghosh et al. 2013); the dark blue arrow indicates fractionation during microbial reduction of Hg(II) and demethylation of MeHg (Kritee et al. 2007, 2009); the light green arrow indicates fractionation during Hg binding to thiol ligands and Hg sorption to iron oxides (Jiskra et al. 2012, Wiederhold et al. 2010); the dark green arrow indicates fractionation during methylation of Hg(II) by sulfate-reducing bacteria (Rodriguez-Gonzalez et al. 2009); the red arrow indicates fractionation during photochemical demethylation of MeHg from aqueous solutions (MIF due to the magnetic isotope effect) (Bergquist & Blum 2007); the orange arrow indicates fractionation during photochemical reduction of Hg(II) from aqueous solutions (MIF due to the magnetic isotope effect) (Bergquist & Blum 2007, Zheng & Hintelmann 2010); the magenta arrow indicates fractionation during photochemical reduction of Hg(II) from snow crystals (MIF due to the magnetic isotope effect) (Sherman et al. 2010); and the purple arrow indicates fractionation due to artificial light–induced Hg(II) reduction via thiol ligands (MIF due to the magnetic isotope effect) (Zheng & Hintelmann 2010). Abbreviations: MIF, mass-independent fractionation; NIST SRM 3133, National Institute of Standards and Technology Standard Reference Material 3133.

METHODS

Criteria for Inclusion of Data

We restricted the publications used in this data compilation and review to journal articles and book chapters accepted for publication before July 15, 2013 that reported Hg isotope ratios of

environmental samples. We also publish herein Hg isotopic data from our laboratory (University of Michigan) for several rock formations and moss samples that have been reported only in meeting abstracts or are unpublished, and additional isotope ratios measured during several studies from our laboratory wherein only a subset of the ratios were originally reported. All of these previously unpublished data are included in **Supplemental Table 1** (follow the **Supplemental Material link** in the online version of this article or at **http://www.annualreviews.org/**).

Supplemental Material

Before including data in this review, we felt that it was important to carefully consider the quality control that was used for the data reported in each publication. To assess the quality of a given data set we followed the common practice in nontraditional stable isotope studies of considering both the variability of internal analytical Hg standards (such as the UM-Almadén standard) and the variability of external procedural standards and/or sample replicates. We used the following criteria to group published Hg isotope data into three categories:

1. Both internal and external standard analyses are reported. The uncertainty of internal standards is $\leq \pm 0.20‰$ (2 SD), and the uncertainty of external standards is $\leq \pm 0.30‰$ (2 SD).
2. Either (*a*) internal or external standard analyses are not reported or (*b*) uncertainty of the internal standards is $> \pm 0.20‰$ (2 SD) or uncertainty of the external standards is $> \pm 0.30‰$ (2 SD).
3. Either (*a*) neither analyses of internal standards nor analyses of external standards are reported or (*b*) no analyses of internal standards are reported, and the uncertainty of external standards is $> \pm 0.30‰$ (2 SD).

To increase confidence in the quality of the data, we included only data from categories 1 and 2 on figures in this compilation. Although some of the category 3 data sets may be of high quality, we could not assess those data sets that did not report measurement of standards (Das et al. 2009; Feng et al. 2010; Foucher & Hintelmann 2006; Ghosh et al. 2008; Hintelmann & Lu 2003; Jackson et al. 2004, 2013). In addition, and as described above, data published by Jackson and coauthors (2004, 2008, 2012, 2013) are not referenced to NIST SRM 3133 or any other widely used reference material and are reported using ratios with ^{202}Hg (instead of ^{198}Hg) in the denominator. Data published by Ghosh et al. (2008) and Das et al. (2009) are also not presented relative to mass ^{198}Hg and cannot be converted to standard isotope ratios for comparison. For these reasons, data from these studies cannot be compared directly with the rest of the data in this compilation and were placed in category 3.

To assist comparisons between studies, we strongly suggest the following guidelines for data reporting as originally outlined in Blum & Bergquist (2007):

1. Isotope ratios should use mass ^{198}Hg in the denominator and be presented relative to either NIST SRM 3133 or some material that has been very well characterized relative to NIST SRM 3133. If an alternate material is used, results from NIST SRM 3133 measured as an internal standard should be presented.
2. Results for both internal and external standards should be presented along with analytical uncertainties for each isotope ratio.
3. Publications should present all measured Hg isotope ratio data (i.e., δ^{196}Hg, δ^{199}Hg, δ^{200}Hg, δ^{202}Hg, δ^{204}Hg) for standards (internal and external) as well as samples. With complete isotope ratio data, elucidation of novel fractionation mechanisms expressed as MIF (i.e., Δ^{199}Hg, Δ^{200}Hg, Δ^{201}Hg, and Δ^{204}Hg) will be facilitated.

Definition of Data Groupings

To make broad comparisons between sample types, we grouped all category 1 and 2 data (1,548 individual analyses) according to the type of sample that was analyzed. We defined eight general

sample types that have been commonly analyzed (herein called groups), and we identified subdivisions of sample types within these groups (herein called subgroups). These groups (with subgroups in parentheses) are: (*a*) geological materials (rocks; Hg ores, minerals, and hydrothermal precipitates; coals); (*b*) sediments (freshwater preanthropogenic, marine preanthropogenic, freshwater anthropogenic with mixed Hg sources, marine anthropogenic with mixed Hg sources, freshwater and marine influenced directly by an anthropogenic point source); (*c*) soils; (*d*) atmospheric samples [rainfall, rainfall influenced directly by coal combustion, total gaseous Hg (TGM), Arctic snow and ice, non-Arctic snow]; (*e*) fish and invertebrates (freshwater fish, invertebrates, estuarine fish, marine near-shore fish, marine open-ocean fish); (*f*) seabird egg contents; (*g*) humans (hair from artisanal gold miners, hair from nonminers, urine from nonminers); and (*h*) vegetation (foliage and leaf litter, tree lichens, Spanish moss). In all of the figures presented in this review, we use a consistent color for each group with different symbols for the various subgroups.

LARGE-MAGNITUDE VARIATIONS IN MERCURY ISOTOPIC COMPOSITION

More than 50 research articles have been published that present Hg isotope ratios of environmental samples. The most important and widely used plot for exploring Hg isotopic variability is that of Δ^{199}Hg (MIF) versus δ^{202}Hg (MDF). As shown in **Figure 2**, the observed variability in the Hg isotopic composition of natural materials is very large. In this review, by grouping data sets on the basis of sample type and examining only the large-scale trends, we necessarily gloss over a wealth of information obtained from Hg isotope variations at individual sites. Many important scientific findings have been based on relatively small differences between samples in δ^{202}Hg and Δ^{199}Hg ($<\sim$0.5‰). We do not mean to downplay the importance of each individual study, but instead we seek here to focus on a global view of large-magnitude variations in environmental Hg isotopic composition. In the sections that follow we explore the observed range in Hg isotopic composition, progressively stepping through the data from large-scale trends to smaller-scale variations, as we sequentially peel back the data in a manner analogous to peeling the layers of an onion.

As shown in **Figure 2**, the total observed range in the Hg isotopic composition of natural materials is >10‰ for Δ^{199}Hg and >8‰ for δ^{202}Hg. The median of the data cluster in **Figure 2** is at $\Delta^{199}\text{Hg} = 0.06‰$ (1 SD = 0.83‰, $n = 1{,}548$) and $\delta^{202}\text{Hg} = -0.62‰$ (1 SD = 1.0‰, $n = 1{,}548$). This median Δ^{199}Hg value is independent of the standard reference material (i.e., NIST SRM 3133) and simply indicates that approximately the same number of samples have been measured with positive MIF as with negative MIF. However, the numerical value of the observed median δ^{202}Hg is controlled by the choice of NIST SRM 3133, which is a metallic Hg product that was mined and purified, as the reference standard. Coincidentally, the commonly reported internal Hg standard, UM-Almadén, which is a metallic Hg product from the Almadén Hg mine in Spain, has an isotopic composition close to the median δ^{202}Hg value for all category 1 and 2 data (UM-Almadén $\delta^{202}\text{Hg} = -0.54 \pm 0.08‰$; Blum & Bergquist 2007).

The overall shape of the cluster of data shown in **Figure 2** is revealing in that it forms a central group with four branches trending in different directions. The symbols trending toward high positive Δ^{199}Hg values represent aquatic organisms including marine open-ocean fish, freshwater fish, and invertebrates. Many studies suggest that these organisms have acquired variably positive Δ^{199}Hg values from microbially produced MeHg that was photochemically degraded to differing extents (Bergquist & Blum 2007, Gehrke et al. 2011b, Kwon et al. 2012, Laffont et al. 2009, Perrot et al. 2010, Point et al. 2011, Senn et al. 2010, Sherman & Blum 2013, Tsui et al. 2013). This photochemical process produces Hg(0) with lower Δ^{199}Hg values than that of the original MeHg and, therefore, results in a residual pool of nondegraded MeHg with higher Δ^{199}Hg values.

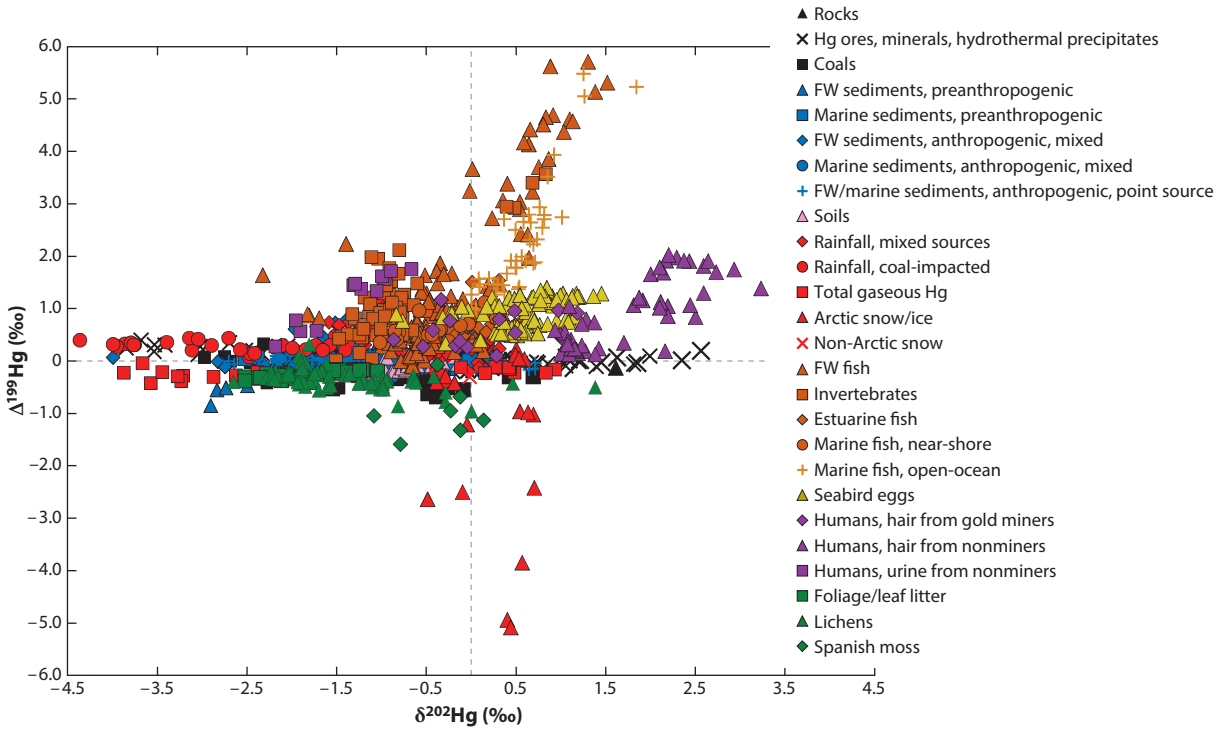

Figure 2

Plot of Δ^{199}Hg versus δ^{202}Hg for all category 1 and 2 data. For a subset of data points from Smith et al. (Smith 2010; Smith et al. 2005, 2008), Biswas et al. (2008), and Bergquist & Blum (2007), Δ^{201}Hg rather than Δ^{199}Hg values were plotted because mass ^{199}Hg was not measured and the Δ^{199}Hg/Δ^{201}Hg ratio in these samples is expected to be close to 1.0. Each data group is represented by a particular color and each subgroup by a particular symbol, as follows: (*a*) Geological materials are shown in black, with rocks as triangles (Blum & Anbar 2010, North 2011, Smith et al. 2008); Hg ores, minerals, and hydrothermal precipitates as crosses (Cooke et al. 2013; Foucher et al. 2009; Sherman et al. 2009; Smith 2010; Smith et al. 2005, 2008; Sonke et al. 2010; Stetson et al. 2009; Yin et al. 2013c); and coals as squares (Biswas et al. 2008, Lefticariu et al. 2011, Sherman et al. 2012b, Sun et al. 2013). (*b*) Sediments are shown in blue, with freshwater (FW) preanthropogenic sediments as triangles (Cooke et al. 2013, Donovan et al. 2013, Gray et al. 2013), marine preanthropogenic sediments as squares (Foucher et al. 2009, Gehrke et al. 2009, Mil-Homens et al. 2013), freshwater sediments with mixed anthropogenic Hg sources as diamonds (Bartov et al. 2013, Cooke et al. 2013, Day et al. 2012, Donovan et al. 2013, Foucher et al. 2013, Gehrke et al. 2011a, Gray et al. 2013, Liu et al. 2011, Perrot et al. 2010, Sherman & Blum 2013, Sonke et al. 2010, Yin et al. 2013c), marine anthropogenic sediments with mixed anthropogenic Hg sources as circles (Mil-Homens et al. 2013, Senn et al. 2010), and freshwater and marine sediments influenced directly by an anthropogenic point source as pluses (Bartov et al. 2013; Cooke et al. 2013; Donovan et al. 2013; Foucher et al. 2009, 2013; Gray et al. 2013; Ma et al. 2013; Perrot et al. 2010; Sonke et al. 2010; Yin et al. 2013b,c). (*c*) Soils are shown as light pink triangles (Biswas et al. 2008, Demers et al. 2013, Estrade et al. 2011, Tsui et al. 2012). (*d*) Atmospheric samples are shown in red, with rainfall influenced by a mixture of sources as diamonds (Chen et al. 2012, Demers et al. 2013, Donovan et al. 2013, Gratz et al. 2010, Sherman et al. 2012b), rainfall influenced directly by a coal-fired power plant as circles (Sherman et al. 2012b), total gaseous Hg as squares (Demers et al. 2013, Gratz et al. 2010, Rolison et al. 2013, Sherman et al. 2010, Yin et al. 2013a), Arctic snow and ice as triangles (Sherman et al. 2010, 2012a), and non-Arctic snow as crosses (Chen et al. 2012). (*e*) Fish and invertebrates are shown in orange, with freshwater fish as triangles (Bergquist & Blum 2007; Kwon et al. 2012; Laffont et al. 2009; Perrot et al. 2010, 2012; Sherman & Blum 2013; Tsui et al. 2012), invertebrates as squares (Perrot et al. 2010, 2012; Tsui et al. 2012, 2013), estuarine fish as diamonds (Gehrke et al. 2011b), marine near-shore fish as circles (Senn et al. 2010), and marine open-ocean fish as pluses (Blum et al. 2013, Senn et al. 2010). (*f*) Seabird egg contents are shown as dark yellow triangles (Day et al. 2012, Point et al. 2011). (*g*) Samples from humans are shown in purple, with hair from artisanal gold miners as diamonds (Laffont et al. 2011), hair from nonminers as triangles (Laffont et al. 2009, 2011; Sherman et al. 2013), and urine from nonminers as squares (Sherman et al. 2013). (*h*) Vegetation is shown in green, with foliage and leaf litter as squares (Demers et al. 2013, Tsui et al. 2012), tree lichens as triangles (Blum et al. 2012, Carignan et al. 2009, Estrade et al. 2010, Yin et al. 2013a), and Spanish moss as diamonds (Das et al. 2012; L.S. Sherman, J.D. Blum, G.J. Keeler, J.D. Demers & J.T. Dvonch, unpublished manuscript).

Researchers have related the measured Δ^{199}Hg values in organisms to the fraction of the MeHg that was lost due to photochemical demethylation prior to incorporation of the remaining MeHg into the base of the food web (Bergquist & Blum 2007, Blum et al. 2013, Senn et al. 2010, Sherman & Blum 2013, Tsui et al. 2013). For example, the maximum Δ^{199}Hg value on **Figure 2** is for flying fish from the Pacific Ocean, and their Δ^{199}Hg value corresponds to photochemical demethylation of ~80% of the original MeHg (Blum et al. 2013). The magnitude of photochemical demethylation has been related to water depth in the ocean (Blum et al. 2013), water clarity in lakes (Gantner et al. 2009, Sherman & Blum 2013), and the amount of shading by forest canopy in rivers (Tsui et al. 2012).

The other types of samples that display high positive Δ^{199}Hg values are animal tissues that contain MeHg obtained through the consumption of fish. These include seabird egg contents (Day et al. 2012, Point et al. 2011) and human hair (Laffont et al. 2009, 2011; Sherman et al. 2013) (**Figure 2**). Experimental studies indicate that MIF does not occur in the absence of sunlight (i.e., within organisms) or during microbial processes (Kritee et al. 2007, 2009, 2012; Rodriguez-Gonzalez et al. 2009). Therefore, the positive Δ^{199}Hg values observed in birds and humans are believed to be inherited unchanged from MeHg in fish. In contrast, recent studies suggest that MDF does occur within mammals, resulting in higher δ^{202}Hg values in human hair than in the fish that they consume (Laffont et al. 2009, 2011; Sherman et al. 2013). This MDF may be due to the retention of isotopically heavier MeHg in human hair as a result of the preferential in situ demethylation and excretion of isotopically light MeHg (Sherman et al. 2013). Supporting this hypothesis is the observation that demethylated Hg excreted in human urine has lower δ^{202}Hg values than those found in hair samples from the same individuals (Sherman et al. 2013). In contrast, a similar magnitude of in situ MDF has not been observed in freshwater or marine fish tissues (Kwon et al. 2012, 2013). Further research is needed to identify the mechanism(s) responsible for in situ MDF in mammals and to explain its absence in fish.

In contrast to positive MIF, very few sample types exhibit large negative MIF. As shown in **Figure 2**, highly negative Δ^{199}Hg values have been observed only in snow samples from the Arctic collected during atmospheric mercury depletion events (Sherman et al. 2010). During these events, Hg(0) in the atmosphere is oxidized by marine halogens and deposited as Hg(II) associated with halogens on snow crystals. Subsequent photochemical reactions can reduce Hg(II) in the snow to Hg(0), which is released back to the atmosphere (Dommergue et al. 2003, Johnson et al. 2008, Lalonde et al. 2002). Sherman et al. (2010) discovered that the odd-mass-number isotopes of Hg are preferentially reduced and emitted as Hg(0). As a result, the residual Hg(II) in the snowpack displays highly negative Δ^{199}Hg values (Sherman et al. 2010). Tree lichens, Spanish moss, and deciduous foliage samples similarly display negative Δ^{199}Hg values, but of a lesser magnitude (Blum et al. 2012, Carignan et al. 2009, Das et al. 2012, Demers et al. 2013, Estrade et al. 2010, Tsui et al. 2012; L.S. Sherman, J.D. Blum, G.J. Keeler, J.D. Demers & J.T. Dvonch, unpublished manuscript). It was originally suggested that the negative Δ^{199}Hg values observed in lichen samples were representative of the isotopic composition of total gaseous Hg [TGM, primarily Hg(0)] in the atmosphere (Carignan et al. 2009, Estrade et al. 2010). However, subsequent isotopic analyses of background atmospheric TGM demonstrated that this reservoir does not display large negative MIF (Demers et al. 2013, Gratz et al. 2010, Sherman et al. 2010). Zheng & Hintelmann (2010) demonstrated experimentally that photochemical reduction of Hg(II) bound to thiol ligands in aqueous media can cause the preferential release of the odd-mass-number isotopes of Hg, therefore producing negative MIF in the retained fraction. This mechanism has been invoked (Blum et al. 2012, Demers et al. 2013) to explain how Hg(II) deposited from the atmosphere to foliage surfaces can subsequently develop the observed negative MIF signatures, and may provide a general explanation for the negative Δ^{199}Hg values measured in foliage, lichens, and Spanish moss.

In addition to the variability in MIF, a large range in δ^{202}Hg values (MDF) has been observed in environmental samples (**Figure 2**). Highly negative δ^{202}Hg values (<−3.0‰) have been measured primarily in atmospheric samples collected near anthropogenic Hg point sources (Rolison et al. 2013, Sherman et al. 2012b, Yin et al. 2013a). Rainfall collected directly downwind of a coal-fired power plant displayed negative δ^{202}Hg values and slightly positive Δ^{199}Hg values (Sherman et al. 2012b), whereas TGM collected near both a coal-fired power plant and a contaminated Hg mining region displayed negative δ^{202}Hg values and slightly negative Δ^{199}Hg values (Rolison et al. 2013, Yin et al. 2013a). Sun et al. (2013) demonstrated that the light isotopes of Hg are preferentially adsorbed to fly ash particles within coal-fired power plants. The highly negative δ^{202}Hg values observed in atmospheric Hg samples collected downwind from these sources may therefore be the result of the incorporation of fly ash–associated $Hg_{(p)}$ that displays negative δ^{202}Hg values (Sherman et al. 2012b, Sun et al. 2013).

SMALLER-MAGNITUDE VARIATIONS IN MERCURY ISOTOPIC COMPOSITION

Now that we have explored the underlying processes that are responsible for the observed large-scale variability in MIF and MDF that has been reported in natural materials, we explore more subtle Hg isotopic variations. To do this, we first remove from consideration those samples contributing to the most extreme variations. **Figure 3** is a plot of Δ^{199}Hg versus δ^{202}Hg without the data from atmospheric samples collected near anthropogenic point sources, Arctic snow, fish, invertebrates, bird egg contents, human hair and urine, and Spanish moss. Note that the y-axis scale (Δ^{199}Hg) in **Figure 3** has been compressed dramatically compared with that in **Figure 2**, but the x-axis scale (δ^{202}Hg) remains the same.

As shown in **Figure 3**, samples of Hg ores, minerals, and hydrothermal precipitates display a relatively narrow range of Δ^{199}Hg values (<0.4‰) but a very wide range of δ^{202}Hg values. Studies of modern hydrothermal and volcanic systems (Sherman et al. 2009; Smith et al. 2005, 2008; Zambardi et al. 2009) have shown that redox transformations during vapor phase transport and venting of hydrothermal fluids can cause large MDF. These same processes are likely responsible for the preserved variability in δ^{202}Hg values in fossil hydrothermal systems and Hg ores. The small but significant positive Δ^{199}Hg values observed in some Hg deposits may be ascribed to photochemical processes occurring at the surface (e.g., in hot spring pools) and/or inheritance of the MIF signature of Hg leached from sedimentary rocks (Sherman et al. 2009).

The group of samples with the highest Δ^{199}Hg values in **Figure 3** is precipitation (rainfall and snow) that was not directly impacted by a local anthropogenic point source of Hg (Chen et al. 2012, Demers et al. 2013, Donovan et al. 2013, Gratz et al. 2010, Sherman et al. 2012b). Gratz et al. (2010) suggested that photochemical reduction of Hg(II) in raindrops may cause positive MIF in a manner similar to that observed in aqueous systems (Bergquist & Blum 2007). The positive Δ^{199}Hg values observed in rainfall are the result of preferential retention of the odd-mass-number isotopes of Hg in droplets. TGM collected in areas not impacted by a point source has a narrow range in Hg isotopic composition with slightly negative Δ^{199}Hg values (0 to −0.2‰) and slightly positive δ^{202}Hg values (<0.5‰) (Demers et al. 2013, Gratz et al. 2010, Sherman et al. 2010). It is possible that photochemical reduction of Hg from aqueous solutions, photochemical oxidation of Hg(0) in the atmosphere, and mixing of different sources of gaseous Hg result in this observed isotopic composition.

Terrestrial plants take up and store atmospheric TGM through their stomata (Demers et al. 2013). As shown in **Figure 3**, deciduous foliage and lichens are primarily characterized by negative Δ^{199}Hg and δ^{202}Hg values. As described above, the observed negative MIF is most likely caused

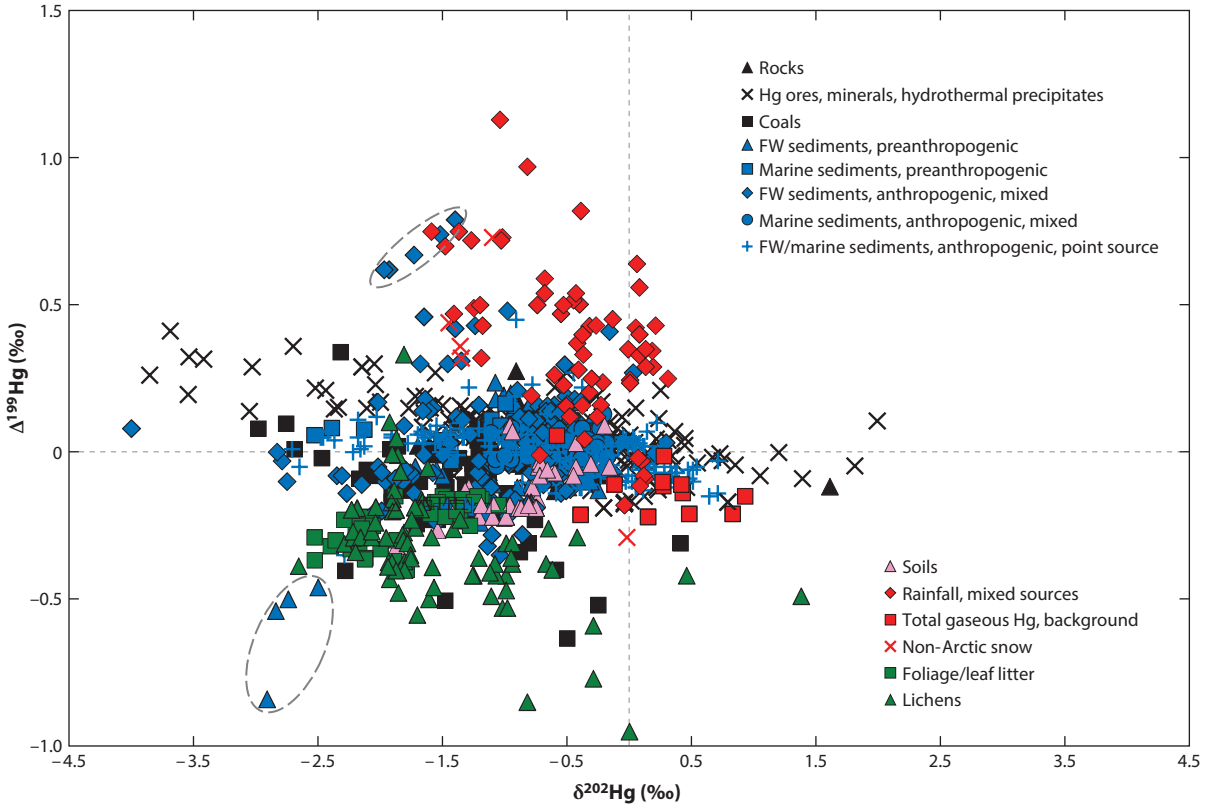

Figure 3

Plot of Δ^{199}Hg versus δ^{202}Hg for a subset of data, with data exhibiting large-magnitude MIF excluded. Data sets are the same as in **Figure 2** excluding those for atmospheric samples collected near anthropogenic point sources, Arctic snow, fish, invertebrates, bird egg contents, human hair and urine, and Spanish moss. Background total gaseous Hg samples are from Demers et al. (2013), Gratz et al. (2010), and Sherman et al. (2010). Dashed gray ovals encompass sediment samples that display outlier Δ^{199}Hg values (Das et al. 2012, Gray et al. 2013). Abbreviation: FW, freshwater.

by photochemical reduction and loss of some Hg from the foliage (Blum et al. 2012, Demers et al. 2013). More negative δ^{202}Hg values in foliage than in background atmospheric TGM (**Figure 3**) have been attributed by Demers et al. (2013) to negative MDF that occurs during the uptake and subsequent oxidation of atmospheric TGM. A similar process likely applies to lichens and mosses. Coal deposits, which are composed of fossilized terrestrial organic matter, also display negative Δ^{199}Hg and δ^{202}Hg values that are inherited, at least in part, from foliage (Biswas et al. 2008). Finally, soils display slightly negative Δ^{199}Hg and δ^{202}Hg values, which likely represent a mixture between foliage litter fall and Hg in soil minerals (Biswas et al. 2008, Demers et al. 2013, Estrade et al. 2011).

The largest groups of samples in **Figure 3** are lake and ocean sediments. These analyses form a dense oval centered at a mean value of $\Delta^{199}\text{Hg} = 0.01‰$ (1 SD = 0.15‰, $n = 436$) and $\delta^{202}\text{Hg} = -0.84‰$ (1 SD = 0.72‰, $n = 436$). A few freshwater sediments display extreme outlier Δ^{199}Hg values. The sediments with high Δ^{199}Hg values (>0.5‰) are salt marsh surface sediments from a barrier island (Das et al. 2012). The authors suggested that the Hg in these surface sediments has undergone in situ photochemical reduction, which may explain the observed positive MIF in

these samples (Das et al. 2012). The outlier sediments with low Δ^{199}Hg values (<−0.45‰) are preanthropogenic sediments from a deep lake core (Gray et al. 2013). We speculate that Hg in these sediments could be associated with the deposition of terrestrial organic matter (derived partly from foliage) from the surrounding watershed, which may explain the observed negative Δ^{199}Hg values. These two groups of outlier samples are excluded from consideration in the subsequent section.

Mercury Isotopic Composition of Rocks and Sediments

An increasingly common application of Hg isotopes is to fingerprint the isotopic composition of a contaminant and trace its movement and chemical transformations in the environment (e.g., Bartov et al. 2013; Cooke et al. 2013; Foucher et al. 2009, 2013; Ma et al. 2013; Sonke et al. 2010). Because Hg is very particle reactive, it is largely sorbed to organic matter or minerals in aquatic systems (Brigham et al. 2009) and is therefore transported and deposited with sediments. Consequently, before initiating a Hg isotope contaminant tracer study, researchers commonly ask what the expected variability in Hg isotopic composition is for the background sediment. **Figure 4** explores this question by further zooming in the scale relative to that in **Figure 3** and plotting only

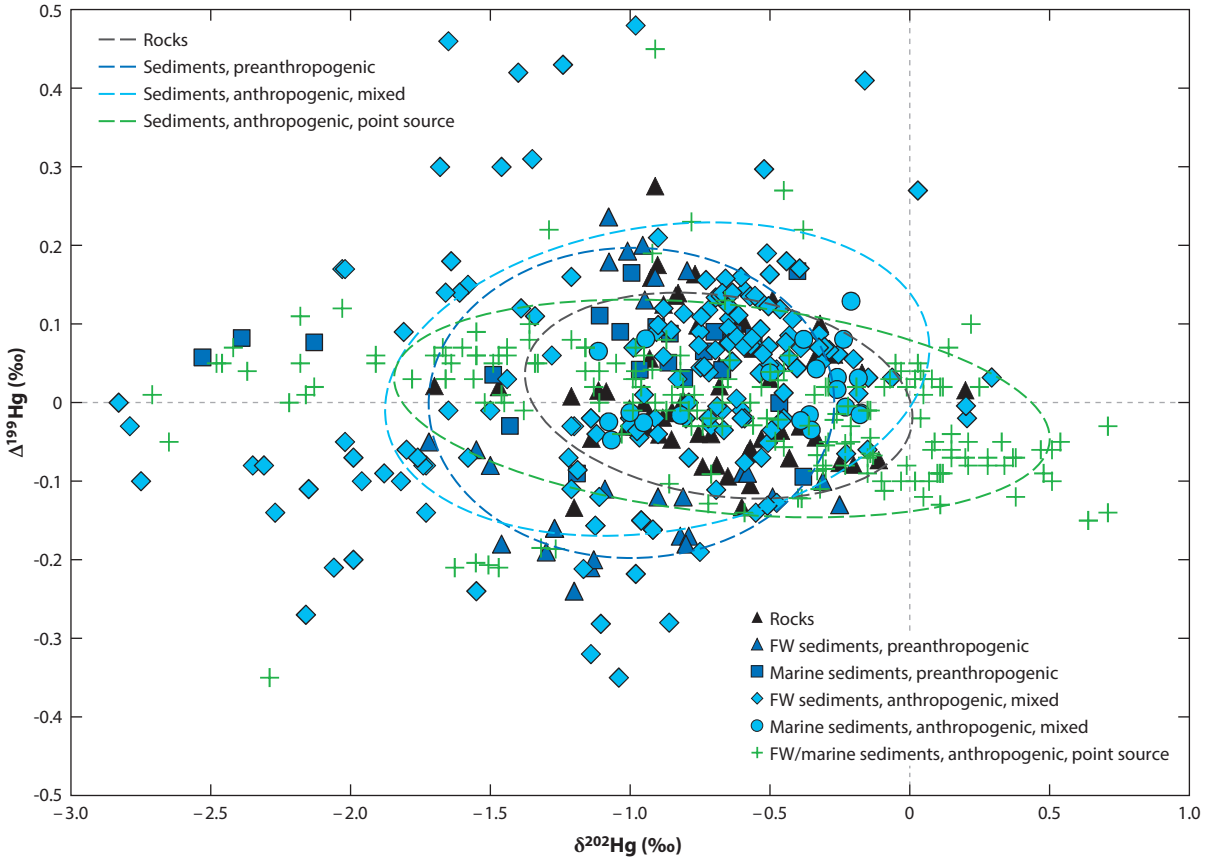

Figure 4

Plot of Δ^{199}Hg versus δ^{202}Hg for rocks and sediments. Included data sets are the same as in **Figure 3**; outlier samples in dashed ovals on **Figure 3** are excluded. Ovals on this diagram depict 1-SD error ellipses around the mean value for each sample subgroup. Abbreviation: FW, freshwater.

analyses of rocks and sediments. A high density of data near the origin obscures the distribution of points associated with any single subgroup of samples. Although mean values (±1 SD) of Δ^{199}Hg and δ^{202}Hg for each sample group give some sense of the extent to which the data overlap, greater clarity is obtained by plotting error ellipses (Ludwig 2007) based on the data. Each ellipse plotted on **Figure 4** bounds an area that defines 67% of the variability associated with samples from each subgroup, and rotation of ellipse major and minor axes reflects the degree to which subgroup variability is associated with either parameter.

Volcanic, metamorphic, and sedimentary rocks ranging in age from the Tertiary to the Archean (**Figure 4**) generally do not display significant levels of MIF (mean Δ^{199}Hg = 0.01‰, 1 SD = 0.09‰, n = 58). The lack of MIF in volcanic and metamorphic rocks supports the hypothesis that large-magnitude MIF occurs only during photochemical reactions in surface environments. Additionally, the observation of no significant MIF in sedimentary rocks may suggest that Hg in these rocks is a mixture of Hg from different reservoirs (e.g., atmospheric, organic matter, minerals) with complementary MIF signatures that average to near zero. In contrast, sedimentary rocks vary significantly in δ^{202}Hg values, with a mean δ^{202}Hg value of −0.68 ± 0.45‰ (1 SD, n = 58). This supports the suggestion that MDF occurs during many geological processes, such as hydrothermal reactions, sorption/desorption, organic matter burial, and diagenesis.

Many researchers have explored Hg isotope variability in both preanthropogenic and anthropogenically impacted sediments. Marine and freshwater sediments (recovered from cores) that were deposited before modern increases in anthropogenic Hg emissions (i.e., pre-1850) display limited MIF (mean Δ^{199}Hg = 0.00‰, 1 SD = 0.13‰, n = 51) and a moderate range in δ^{202}Hg values (mean = −1.00‰, 1 SD = 0.48‰, n = 51). Younger marine and freshwater surface sediments that were influenced by anthropogenic sources, but not directly associated with a point source of Hg contamination, have similar but more highly variable Δ^{199}Hg values (mean = 0.03‰, 1 SD = 0.13‰, n = 191) and δ^{202}Hg values (mean = −0.91‰, 1 SD = 0.64‰, n = 191). Finally, freshwater and marine surface sediments that are associated with point sources of Hg contamination have a similar range in Δ^{199}Hg values (mean = −0.01‰, 1 SD = 0.09‰ n = 185) but have a wider range of δ^{202}Hg values (mean = −0.67‰, 1 SD = 0.78‰, n = 185). In particular, some point source–contaminated sediments associated with Hg mining and metal smelting can be readily differentiated from the other sediments by their high positive δ^{202}Hg values (Foucher et al. 2013, Sonke et al. 2010). In many individual case studies, sediments contaminated by point sources are isotopically distinct from local background sediment even though the full data ranges for these two groups of sediments overlap. Thus, a case-by-case assessment must be made to determine whether the isotopic composition of point source pollution is distinguishable from that of background sediments.

THE Δ^{199}Hg/Δ^{201}Hg RATIO

For sample types that display values of Δ^{199}Hg greater than approximately ±0.30‰, it is illustrative to consider Δ^{199}Hg/Δ^{201}Hg ratios. Experimental studies of aqueous solutions with natural organic matter have demonstrated that photochemical reduction of Hg(II) yields residual Hg(II) with a Δ^{199}Hg/Δ^{201}Hg ratio of 1.00 ± 0.01 (1 SE), whereas MeHg photodegradation yields residual MeHg with a Δ^{199}Hg/Δ^{201}Hg ratio of 1.36 ± 0.04 (1 SE) (Bergquist & Blum 2007). As shown in **Figure 5** (with the exception of a few outliers), measured natural samples plot within analytical uncertainty of the bounding Δ^{199}Hg/Δ^{201}Hg ratios of 1.00 and 1.36. Marine fish plot at an average Δ^{199}Hg/Δ^{201}Hg ratio of 1.20 ± 0.01 (1 SE, n = 60), and the hair of humans and eggs of seabirds that eat marine fish also plot on a line with slope 1.20 ± 0.02 (1 SE, n = 134). Freshwater fish display slightly higher and more variable Δ^{199}Hg/Δ^{201}Hg ratios

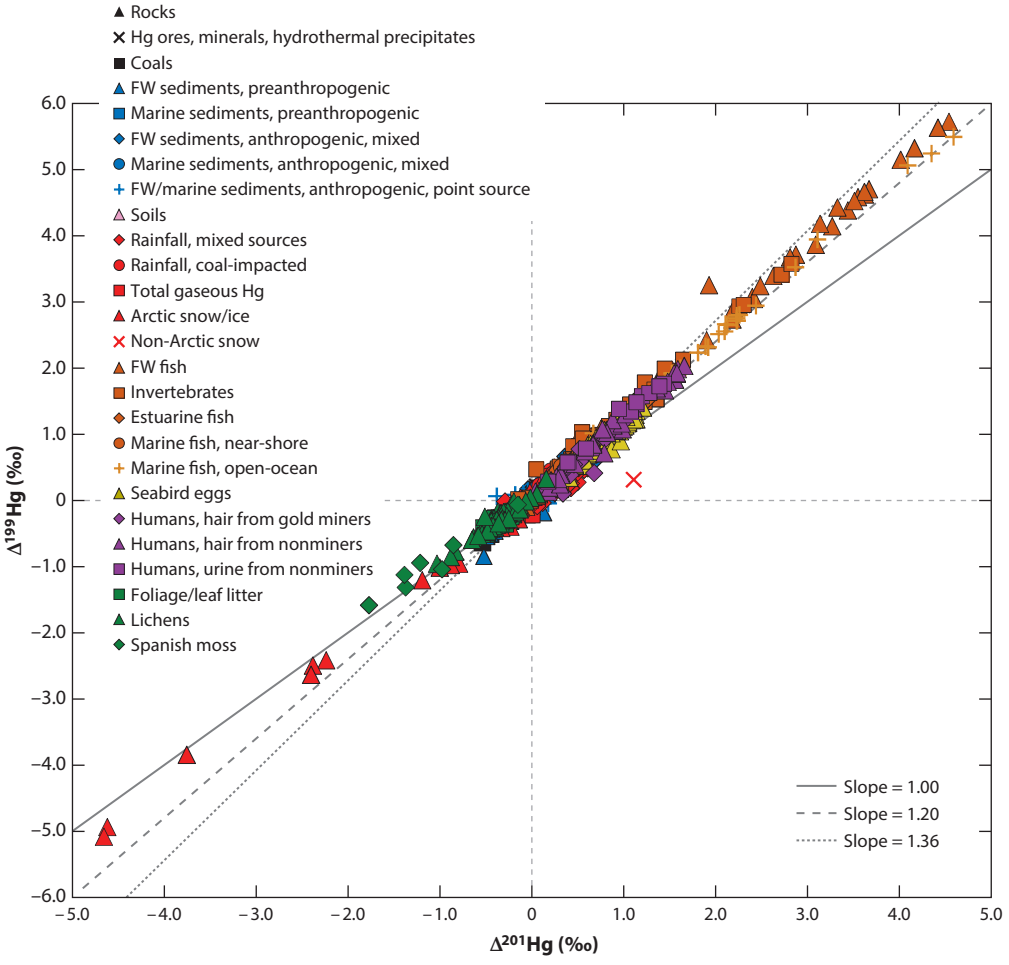

Figure 5

Plot of Δ^{199}Hg versus Δ^{201}Hg for all included data (data sets are the same as in **Figure 2**). Because mass ^{199}Hg was not analyzed in some early studies, a subset of data points from Smith et al. (Smith 2010; Smith et al. 2005, 2008), Biswas et al. (2008), and Bergquist & Blum (2007) are not plotted on this figure. The solid line indicates a slope of 1.00, the dashed line a slope of 1.20, and the dotted line a slope of 1.36. Note that all of the geological material data points are hidden behind those for other sample types. Abbreviation: FW, freshwater.

that may depend on the chemical characteristics of specific water bodies (overall $\Delta^{199}\text{Hg}/\Delta^{201}\text{Hg} = 1.28$, 1 SE = 0.01, $n = 135$). Although MIF results from the photochemical degradation of MeHg in both freshwater and marine systems, it is interesting that slightly lower $\Delta^{199}\text{Hg}/\Delta^{201}\text{Hg}$ ratios have been observed in marine organisms. This may be due to the influence of differences in organic matter and/or dissolved cations and halogens in seawater, and warrants further study.

As described above, lichen, Spanish moss, and Arctic snow display negative Δ^{199}Hg and Δ^{201}Hg values. Most of these samples have $\Delta^{199}\text{Hg}/\Delta^{201}\text{Hg}$ ratios within analytical uncertainty of the bounding slopes of 1.0 and 1.2 (**Figure 5**). Other sample types that display less, but still significant, MIF (e.g., $> \pm 0.3$‰), including rainfall, foliage, sediments, and coals, have $\Delta^{199}\text{Hg}/\Delta^{201}\text{Hg}$ ratios

close to 1.0. These data support the hypothesis that MIF is caused by photochemical reduction of Hg(II) from these materials. However, scatter in the data for these low MIF samples makes it difficult to distinguish between slopes ranging from 0.8 to 1.2.

MASS-INDEPENDENT FRACTIONATION OF THE EVEN-MASS-NUMBER MERCURY ISOTOPES

In addition to large MIF of the odd-mass-number isotopes of Hg (^{199}Hg and ^{201}Hg), several recent studies have reported MIF of the even-mass-number isotopes (^{200}Hg and ^{204}Hg) (Chen et al. 2012, Demers et al. 2013, Gratz et al. 2010, Sherman et al. 2012b). As discussed above, the ^{202}Hg/^{198}Hg ratio is commonly used to express MDF because this ratio gives a large mass difference (4 amu) without the use of ^{196}Hg, which has very low abundance (0.15%), or ^{204}Hg, which has a potential isobaric interference with ^{204}Pb. For the vast majority of samples analyzed, ^{200}Hg has been found to fractionate mass dependently, and thus Δ^{200}Hg is within error of zero. However, a small number of samples, predominantly of atmospheric origin, have Δ^{200}Hg values outside of typical analytical uncertainty (i.e., >0.2‰) (**Figure 6**). To produce this anomaly, an additional MIF mechanism must be influencing the abundance of one or more of the even-mass-number isotopes (i.e., ^{198}Hg, ^{200}Hg, or ^{202}Hg).

Gratz et al. (2010) first documented small Δ^{200}Hg anomalies in precipitation collected in the Great Lakes region, United States. Chen et al. (2012) later measured much larger Δ^{200}Hg anomalies in rain and snow in Ontario, Canada, and suggested that this may be caused by photochemical oxidation of Hg(0) on particle surfaces in the tropopause. In addition, as shown in **Figure 6**, a small number of nonatmospheric samples have significant Δ^{200}Hg anomalies. However, these are all samples that are likely to be strongly influenced by atmospheric Hg, including one Spanish moss sample (L.S. Sherman, J.D. Blum, G.J. Keeler, J.D. Demers & J.T. Dvonch, unpublished manuscript) and several samples from a salt marsh system (Das et al. 2012). The mechanisms believed to produce MIF of the odd-mass-number isotopes of Hg (i.e., the magnetic isotope effect and the nuclear volume effect) are not predicted to result in large-magnitude Δ^{200}Hg anomalies. Nuclear self-shielding, which has been observed in Hg vapor lamps, may be capable of producing Δ^{200}Hg anomalies, but the observed fractionation patterns for all the Hg isotopes are not consistent between atmospheric samples and Hg vapor lamps (Chen et al. 2012, Mead et al. 2013). Even-mass-number MIF is intriguing and may be a useful tracer of upper atmospheric Hg chemistry, but additional research into possible causal mechanisms of the observed anomalies is needed.

CONCLUSIONS

More than a decade of research into the systematics of Hg isotope fractionation and variability among Earth and environmental reservoirs has produced a wealth of data and has significantly enhanced our scientific understanding of Hg biogeochemistry. Hg isotopes have been used to better understand photochemical reaction mechanisms, Hg redox chemistry, and microbial processes. They have also been employed to trace anthropogenic atmospheric emissions and other releases of Hg into sensitive surface environments and to better understand the factors that lead to Hg mobility, bioavailability, and bioaccumulation. Ultimately, Hg isotopes will enable us to better trace sources of Hg to sensitive wildlife and at-risk human populations, and in so doing help to reduce exposure to this potent neurotoxin.

In this review we compile and plot all available data that can be accurately compared to explore the range of Hg isotopic variability observed in geologic and environmental samples.

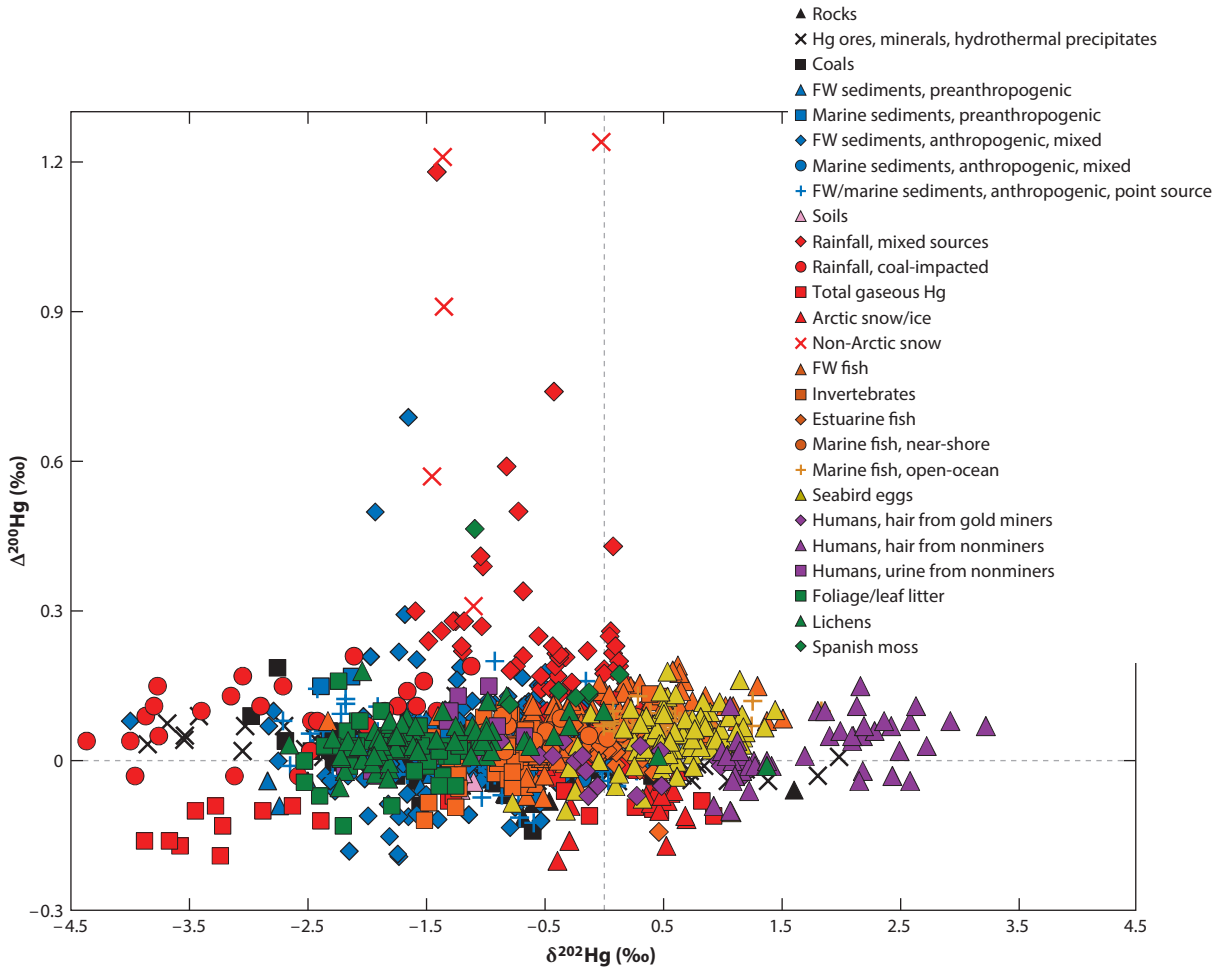

Figure 6

Plot of Δ^{200}Hg versus δ^{202}Hg for all included data (data sets are the same as in **Figure 2**). Abbreviation: FW, freshwater.

This large-scale overview allows us to interpret major trends in Hg isotope data. For instance, we confirm that photochemical reduction of MeHg is likely responsible for the observed large-magnitude positive MIF, whereas photochemical reduction of inorganic Hg is likely responsible for large-magnitude negative MIF. In addition, the largest range in δ^{202}Hg values is observed in geological materials (especially those associated with Hg ore deposits) and rainfall impacted by coal combustion, which indicates that hydrothermal reactions, surface sorption, organic matter burial, and other processes can collectively lead to large MDF.

This compilation also allows us to examine the current gaps in data and in our understanding of Hg isotope systematics. Very few data are available from intrusive or extrusive igneous rock types, which make up large reservoirs of Hg. Fractionation associated with Hg deposition from the atmosphere to the land and ocean surfaces is complex and needs additional research. In particular, significant MDF occurs during the uptake and storage of Hg in foliage. This fractionation needs to be further studied to assess its importance in the global Hg isotope mass balance. Additional

research is also needed to better understand Hg isotope fractionation processes occurring in the atmosphere, including more experimental work to elucidate the mechanisms resulting in the observed MIF of even-mass-number Hg isotopes. Hg isotope geochemistry is only in its adolescence, and as the field matures we expect that Hg isotopes will contribute to a better understanding of virtually every component of the global Hg biogeochemical cycle.

DISCLOSURE STATEMENT

The authors are not aware of any affiliations, memberships, funding, or financial holdings that might be perceived as affecting the objectivity of this review.

ACKNOWLEDGMENTS

Financial support for Hg isotope research over the years at the University of Michigan has come from NSF, DOE, NASA, SFB-RMP, FL-DEP, and internal university funds. The authors are grateful to the Hg isotope biogeochemistry community for their efforts over the past decade to produce high-quality data that can be compared between laboratories and, in so doing, to solidify the importance of Hg isotope research in the critical task of unraveling the complex behavior of Hg in the environment. We especially thank current and past members of our research group for many stimulating discussions about the meaning of Hg isotope variations in the Earth and environment.

LITERATURE CITED

Bartov G, Deonarine A, Johnson TM, Ruhl L, Vengosh A, Hsu-Kim H. 2013. Environmental impacts of the Tennessee Valley Authority Kingston coal ash spill. 1. Source apportionment using mercury stable isotopes. *Environ. Sci. Technol.* 47:2092–99

Bergquist BA, Blum JD. 2007. Mass-dependent and mass-independent fractionation of Hg isotopes by photoreduction in aquatic systems. *Science* 318:417–20

Bergquist BA, Blum JD. 2009. The odds and evens of mercury isotopes: applications of mass-dependent and mass-independent isotope fractionation. *Elements* 5:353–57

Biswas A, Blum JD, Bergquist BA, Keeler GJ, Zhouqing X. 2008. Natural mercury isotope variation in coal deposits and organic soils. *Environ. Sci. Technol.* 42:8303–9

Blum JD. 2011. Applications of stable mercury isotopes to biogeochemistry. In *Handbook of Environmental Isotope Geochemistry*, ed. M Baskaran, pp. 229–45. Berlin: Springer

Blum JD, Anbar AD. 2010. Mercury isotopes in the late Archean Mount McRae Shale. *Geochim. Cosmochim. Acta* 74:A98

Blum JD, Bergquist BA. 2007. Reporting the variations in the natural isotopic composition of mercury. *Anal. Bioanal. Chem.* 388:353–59

Blum JD, Johnson MW, Gleason JD, Demers JD, Landis MS, Krupa S. 2012. Mercury concentration and isotopic composition of epiphytic tree lichens in the Athabasca oil sands region. In *Alberta Oil Sands: Energy, Industry, and the Environment*, ed. KE Percy, pp. 373–90. Dev. Environ. Sci. 11. Amsterdam, Neth.: Elsevier

Blum JD, Popp BN, Drazen JC, Choy CA, Johnson MW. 2013. Evidence for methylmercury production below the mixed layer in the central North Pacific Ocean. *Nat. Geosci.* 6:879–84

Brigham ME, Wentz DA, Aiken GR, Krabbenhoft DP. 2009. Mercury cycling in stream ecosystems. 1. Water column chemistry and transport. *Environ. Sci. Technol.* 43:2720–25

Carignan J, Estrade N, Sonke JE, Donard OFX. 2009. Odd isotope deficits in atmospheric Hg measured in lichens. *Environ. Sci. Technol.* 43:5660–64

Chen J, Hintelmann H, Feng X, Dimock B. 2012. Unusual fractionation of both odd and even mercury isotopes in precipitation from Peterborough, ON, Canada. *Geochim. Cosmochim. Acta* 90:33–46

Cooke CA, Hintelmann H, Ague JJ, Burger R, Biester H, et al. 2013. Use and legacy of mercury in the Andes. *Environ. Sci. Technol.* 47:4181–88

Coplen TB. 2011. Guidelines and recommended terms for expression of stable-isotope-ratio and gas-ratio measurement results. *Rapid Commun. Mass Spectrom.* 25:2538–60

Das R, Bizimis M, Wilson AM. 2012. Tracing mercury seawater vs. atmospheric inputs in a pristine SE USA salt marsh system: mercury isotope evidence. *Chem. Geol.* 336:50–61

Das R, Salters VJM, Odem AL. 2009. A case for in vivo mass-independent fractionation of mercury isotopes in fish. *Geochem. Geophys. Geosyst.* 10:Q11012

Day RD, Roseneau DG, Berail S, Hobson KA, Donard OFX, et al. 2012. Mercury stable isotopes in seabird eggs reflect a gradient from terrestrial geogenic to oceanic mercury reservoirs. *Environ. Sci. Technol.* 46:5327–35

Demers JD, Blum JD, Zak DR. 2013. Mercury isotopes in a forested ecosystem: implications for air-surface exchange dynamics and the global mercury cycle. *Glob. Biogeochem. Cycles* 27:1–17

Dommergue A, Ferrari CP, Gauchard P-A, Boutron CF. 2003. The fate of mercury species in a sub-arctic snowpack during snowmelt. *Geophys. Res. Lett.* 30:1621

Donovan PM, Blum JD, Yee D, Gehrke GE, Singer MB. 2013. An isotopic record of mercury in San Francisco Bay sediment. *Chem. Geol.* 349–50:87–98

Douglas TA, Sturm M, Simpson WR, Blum JD, Alvarez-Aviles L, et al. 2008. Influence of snow and ice crystal formation and accumulation on mercury deposition to the Arctic. *Environ. Sci. Technol.* 42:1542–51

Estrade N, Carignan J, Donard OFX. 2010. Isotope tracing of atmospheric mercury sources in an urban area of northeastern France. *Environ. Sci. Technol.* 44:6062–67

Estrade N, Carignan J, Donard OFX. 2011. Tracing and quantifying anthropogenic mercury sources in soils of northern France using isotopic signatures. *Environ. Sci. Technol.* 45:1235–42

Estrade N, Carignan J, Sonke JE, Donard OFX. 2009. Mercury isotope fractionation during liquid-vapor evaporation experiments. *Geochim. Cosmochim. Acta* 73:2693–711

Evers DC, Han Y-J, Driscoll CT, Kamman NC, Goodale MW, et al. 2007. Biological mercury hotspots in the northeastern United States and southeastern Canada. *Bioscience* 57:29–43

Feng X, Foucher D, Hintelmann H, Yan H, He T, Qiu G. 2010. Tracing mercury contamination sources in sediments using mercury isotope compositions. *Environ. Sci. Technol.* 44:3363–68

Fitzgerald WF, Lamborg CH. 2003. Geochemistry of mercury in the environment. In *Environmental Geochemistry*, ed. HD Holland, KK Turekian, pp. 107–48. Treatise Geochem. 9. Oxford, UK: Elsevier

Foucher D, Hintelmann H. 2006. High-precision measurement of mercury isotope ratios in sediments using cold-vapor generation multi-collector inductively coupled plasma mass spectrometry. *Anal. Bioanal. Chem.* 384:1470–78

Foucher D, Hintelmann H, Al TA, MacQuarrie KT. 2013. Mercury isotope fractionation in waters and sediments of the Murray Brook mine watershed (New Brunswick, Canada): tracing mercury contamination and transformation. *Chem. Geol.* 336:87–95

Foucher D, Ogrinc N, Hintelmann H. 2009. Tracing mercury contamination from the Idrija mining region (Slovenia) to the Gulf of Trieste using Hg isotope ratio measurements. *Environ. Sci. Technol.* 43:33–39

Gantner N, Hintelmann H, Zheng W, Muir DC. 2009. Variations in stable isotope fractionation of Hg in food webs of Arctic lakes. *Environ. Sci. Technol.* 43:9148–54

Gehrke GE, Blum JD, Marvin-DePasquale M. 2011a. Sources of mercury to San Francisco Bay surface sediment as revealed by mercury stable isotopes. *Geochim. Cosmochim. Acta* 75:691–705

Gehrke GE, Blum JD, Meyers PA. 2009. The geochemical behavior and isotopic composition of Hg in a mid-Pleistocene western Mediterranean sapropel. *Geochim. Cosmochim. Acta* 73:1651–65

Gehrke GE, Blum JD, Slotton DG, Greenfield BK. 2011b. Mercury isotopes link mercury in San Francisco Bay forage fish to surface sediments. *Environ. Sci. Technol.* 45:1264–70

Ghosh S, Schauble EA, Couloume GL, Blum JD, Bergquist BA. 2013. Estimation of nuclear volume dependent fractionation of mercury isotopes in equilibrium liquid-vapor evaporation experiments. *Chem. Geol.* 336:5–12

Ghosh S, Xu Y, Humayun M, Odom L. 2008. Mass-independent fractionation of mercury isotopes in the environment. *Geochem. Geophys. Geosyst.* 9:Q03004

Gratz LE, Keeler GJ, Blum JD, Sherman LS. 2010. Isotopic composition and fractionation of mercury in Great Lakes precipitation and ambient air. *Environ. Sci. Technol.* 44:7764–70

Gray JE, Pribil MJ, Van Metre PC, Borrok DM, Thapalia A. 2013. Identification of contamination in a lake sediment core using Hg and Pb isotopic compositions, Lake Ballinger, Washington, USA. *Appl. Geochem.* 29:1–12

Gustin MS, Lindberg SE, Weisberg PJ. 2008. An update on the natural sources and sinks of atmospheric mercury. *Appl. Geochem.* 23:482–93

Hintelmann H. 2012. Use of stable isotopes in mercury research. In *Mercury in the Environment*, ed. MS Bank, pp. 55–71. Berkeley: Univ. Calif. Press

Hintelmann H, Lu S. 2003. High precision isotope ratio measurements of mercury isotopes in cinnabar ores using multi-collector inductively coupled plasma mass spectrometry. *Analyst* 128:635–39

Jackson TA. 2001. Variations in the isotope composition of mercury in a freshwater sediment sequence and food web. *Can. J. Fish. Aquat. Sci.* 58:185–96

Jackson TA, Muir DCG. 2012. Mass-dependent and mass-independent variations in the isotope composition of mercury in a sediment core from a lake polluted by emissions from the combustion of coal. *Sci. Total Environ.* 417–18:189–203

Jackson TA, Muir DCG, Vincent WF. 2004. Historical variations in the stable isotope composition of mercury in Arctic lake sediments. *Environ. Sci. Technol.* 38:2813–21

Jackson TA, Telmer KH, Muir DCG. 2013. Mass-dependent and mass-independent variations in the isotope composition of mercury in cores from lakes polluted by a smelter: effects of smelter emissions, natural processes, and their interactions. *Chem. Geol.* 352:27–46

Jackson TA, Whittle DM, Evans MS, Muir DCG. 2008. Evidence for mass-independent and mass-dependent fractionation of the stable isotopes of mercury by natural processes in aquatic ecosystems. *Appl. Geochem.* 23:547–71

Jiskra M, Wiederhold JG, Bourdon B, Kretzschmar R. 2012. Solution speciation controls mercury isotope fractionation of Hg(II) sorption to goethite. *Environ. Sci. Technol.* 46:6654–62

Johnson CM, Beard BL, Albarede F, eds. 2004. *Geochemistry of Non-Traditional Stable Isotopes*. Rev. Mineral. Geochem. 55. Washington, DC: Mineral. Soc. Am.

Johnson KP, Blum JD, Keeler GJ, Douglas TA. 2008. Investigation of the deposition and emission of mercury in arctic snow during an atmospheric mercury depletion event. *J. Geophys. Res.* 113:D17304

Kritee K, Barkay T, Blum JD. 2009. Mass dependent stable isotope fractionation of mercury during *mer* mediated microbial degradation of monomethylmercury. *Geochim. Cosmochim. Acta* 73:1285–96

Kritee K, Blum JD, Johnson MW, Bergquist BA, Barkay T. 2007. Mercury stable isotope fractionation during reduction of Hg(II) to Hg(0) by mercury resistant microorganisms. *Environ. Sci. Technol.* 41:1889–95

Kritee K, Blum JD, Reinfelder JR, Barkay T. 2012. Microbial stable isotope fractionation of mercury: a synthesis of present understanding and future directions. *Chem. Geol.* 336:13–25

Kwon SY, Blum JD, Carvan MJ, Basu N, Head JA, et al. 2012. Absence of fractionation of mercury isotopes during trophic transfer of methylmercury to freshwater fish in captivity. *Environ. Sci. Technol.* 46:7527–34

Kwon SY, Blum JD, Chirby MA, Chesney EJ. 2013. Application of mercury isotopes for tracing trophic transfer and internal distribution of mercury in marine fish feeding experiments. *Environ. Toxicol. Chem.* 32:2322–30

Laffont L, Sonke JE, Maurice L, Hintelmann H, Pouilly M, et al. 2009. Anomalous mercury isotopic compositions of fish and human hair in the Bolivian Amazon. *Environ. Sci. Technol.* 43:8985–90

Laffont L, Sonke JE, Maurice L, Monrroy SL, Chincheros J, et al. 2011. Hg speciation and stable isotope signatures in human hair as a tracer for dietary and occupational exposure to mercury. *Environ. Sci. Technol.* 45:9910–16

Lalonde J, Poulain AJ, Amyot M. 2002. The role of mercury redox reactions in snow on snow-to-air mercury transfer. *Environ. Sci. Technol.* 36:174–78

Lauretta DS, Klaue B, Blum JD, Buseck PR. 2001. Mercury abundances and isotopic compositions in the Murchison (CM) and Allende (CV) carbonaceous chondrites. *Geochim. Cosmochim. Acta* 65:2807–18

Lefticariu L, Blum JD, Gleason JD. 2011. Mercury isotopic evidence for multiple mercury sources in coal from the Illinois Basin. *Environ. Sci. Technol.* 45:1724–29

Lindberg SE, Brooks S, Lin C-J, Scott KJ, Landis MS, et al. 2002. Dynamic oxidation of gaseous mercury in the Arctic troposphere at polar sunrise. *Environ. Sci. Technol.* 36:1245–56

Liu J, Feng X, Yin R, Zhu W, Li Z. 2011. Mercury distributions and mercury isotope signatures in sediments of Dongjiang, the Pearl River Delta, China. *Chem. Geol.* 287:81–89

Ludwig K. 2007. *Isoplot 3.57, a geochronological toolkit for Microsoft Excel*. Spec. Publ. 4, Berkeley Geochronol. Cent., Berkeley, CA

Ma J, Hintelmann H, Kirk JL, Muir DCG. 2013. Mercury concentrations and mercury isotope composition in lake sediment cores from the vicinity of a metal smelting facility in Flin Flon, Manitoba. *Chem. Geol.* 336:96–102

Mason RP, Fitzgerald WF, Morel FMM. 1994. The biogeochemical cycling of elemental mercury: anthropogenic influences. *Geochim. Cosmochim. Acta* 58:3191–98

Mead C, Lyons JR, Johnson TM, Anbar AD. 2013. Unique Hg stable isotope signatures of compact fluorescent lamp–sourced Hg. *Environ. Sci. Technol.* 47:2542–47

Mil-Homens M, Blum JD, Canario J, Caetano M, Costa AM, et al. 2013. Tracing anthropogenic Hg and Pb input using stable Hg and Pb isotope ratios in sediments of the central Portuguese Margin. *Chem. Geol.* 336:62–71

Morel FMM, Kraepiel AML, Amyot M. 1998. The chemical cycle and bioaccumulation of mercury. *Annu. Rev. Ecol. Syst.* 29:543–66

North S. 2011. *Mercury concentrations and isotopic signature of the Alpine and Otago Schists, New Zealand*. Senior Thesis, Dept. Earth Env. Sci., Univ. Mich.

Perrot V, Epov VN, Pastukhov MV, Grebenshchikova VI, Zouiten C, et al. 2010. Tracing sources and bioaccumulation of mercury in fish of Lake Baikal–Angara River using Hg isotopic composition. *Environ. Sci. Technol.* 44:8030–37

Perrot V, Pastukhov MV, Epov VN, Husted S, Donard OFX, Amouroux D. 2012. Higher mass-independent isotope fractionation of methylmercury in the pelagic food web of Lake Baikal (Russia). *Environ. Sci. Technol.* 46:5902–11

Point D, Sonke JE, Day RD, Roseneau DG, Hobson KA, et al. 2011. Methylmercury photodegradation influenced by sea-ice cover in Arctic marine ecosystems. *Nat. Geosci.* 4:188–94

Porcelli D, Baskaran M. 2011. An overview of isotope geochemistry in environmental studies. In *Handbook of Environmental Isotope Geochemistry*, ed. M Baskaran, pp. 11–32. Berlin: Springer

Ridley WI, Stetson SJ. 2006. A review of isotopic composition as an indicator of the natural and anthropogenic behavior of mercury. *Appl. Geochem.* 21:1889–99

Rodriguez-Gonzalez P, Epov VN, Bridou R, Tessier E, Guyoneaud R, et al. 2009. Species-specific stable isotope fractionation of mercury during Hg(II) methylation by an anaerobic bacteria (*Desulfobulbus propionicus*) under dark conditions. *Environ. Sci. Technol.* 43:9183–88

Rolison JM, Landing WM, Luke W, Cohen M, Salters VJM. 2013. Isotopic composition of species-specific atmospheric Hg in a coastal environment. *Chem. Geol.* 336:37–49

Schroeder WH, Munthe J. 1998. Atmospheric mercury—an overview. *Atmos. Environ.* 32:809–22

Senn DB, Chesney EJ, Blum JD, Bank MS, Maage A, Shine JP. 2010. Stable isotope (N, C, Hg) study of methylmercury sources and trophic transfer in the northern Gulf of Mexico. *Environ. Sci. Technol.* 44:1630–37

Sherman LS, Blum JD. 2013. Mercury stable isotopes in sediments and largemouth bass from Florida lakes, USA. *Sci. Total Environ.* 448:163–75

Sherman LS, Blum JD, Douglas TA, Steffen A. 2012a. Frost flowers growing in the Arctic ocean–atmosphere–sea ice–snow interface: 2. Mercury exchange between the atmosphere, snow, and frost flowers. *J. Geophys. Res.* 117:D00R10

Sherman LS, Blum JD, Franzblau A, Basu N. 2013. New insight into biomarkers of human mercury exposure using naturally occurring mercury stable isotopes. *Environ. Sci. Technol.* 47:3403–9

Sherman LS, Blum JD, Johnson KP, Keeler GJ, Barres JA, Douglas TA. 2010. Mass-independent fractionation of mercury isotopes in Arctic snow driven by sunlight. *Nat. Geosci.* 3:173–77

Sherman LS, Blum JD, Keeler GJ, Demers JD, Dvonch JT. 2012b. Investigation of local mercury deposition from a coal-fired power plant using mercury isotopes. *Environ. Sci. Technol.* 46:382–90

Sherman LS, Blum JD, Nordstrom DK, McCleskey RB, Barkay T, Vetriani C. 2009. Mercury isotopic composition of hydrothermal systems in the Yellowstone Plateau volcanic field and Guaymas Basin sea-floor rift. *Earth Planet. Sci. Lett.* 279:86–96

Smith CN. 2010. *Isotopic geochemistry of mercury in active and fossil hydrothermal systems*. PhD Thesis, Dep. Geol. Sci., Univ. Mich., Ann Arbor

Smith CN, Kesler SE, Blum JD, Rytuba JJ. 2008. Isotope geochemistry of mercury in source rocks, mineral deposits and spring deposits of the California Coast Ranges, USA. *Earth Planet. Sci. Lett.* 269:399–407

Smith CN, Kesler SE, Klaue B, Blum JD. 2005. Mercury isotope fractionation in fossil hydrothermal systems. *Geology* 33:825–28

Sonke JE, Schafer J, Chmeleff J, Audry S, Blanc G, Dupre B. 2010. Sedimentary mercury stable isotope records of atmospheric and riverine pollution from two major European heavy metal refineries. *Chem. Geol.* 279:90–100

Stetson SJ, Gray JE, Wanty RB, Macalady DL. 2009. Isotopic variability of mercury in ore, mine-waste calcine, and leachates of mine-waste calcine from areas mined for mercury. *Environ. Sci. Technol.* 43:7331–36

Sun R, Heimbürger L-E, Sonke JE, Liu G, Amouroux D, Berail S. 2013. Mercury stable isotope fractionation in six utility boilers of two large coal-fired power plants. *Chem. Geol.* 336:103–11

Sunderland EM. 2007. Mercury exposure from domestic and imported estuarine and marine fish in the U.S. seafood market. *Environ. Health Perspect.* 115:235–42

Tsui MTK, Blum JD, Finlay JC, Balogh SJ, Kwon SY, Nollet YH. 2013. Photodegradation of methylmercury in stream ecosystems. *Limnol. Oceanogr.* 58:13–22

Tsui MTK, Blum JD, Kwon SY, Finlay JC, Balogh SJ, Nollet YH. 2012. Sources and transfers of methylmercury in adjacent river and forest food webs. *Environ. Sci. Technol.* 46:10957–64

US EPA. 1997. *Mercury study report to Congress*, Vol. II: *An inventory of anthropogenic mercury emissions in the United States*. EPA-452/R-97-004. Research Triangle Park, NC: EPA OAQPS/ORD

Wiederhold JG, Cramer CJ, Daniel K, Infante I, Bourdon B, Kretzschmar R. 2010. Equilibrium mercury isotope fractionation between dissolved Hg(II) species and thiol-bound Hg. *Environ. Sci. Technol.* 44:4191–97

Yin R, Feng X, Meng B. 2013a. Stable mercury isotope variation in rice plants (*Oryza sativa* L.) from the Wanshan mercury mining district, SW China. *Environ. Sci. Technol.* 47:2238–45

Yin R, Feng X, Shi W. 2010. Application of the stable-isotope system to the study of sources and fate of Hg in the environment: a review. *Appl. Geochem.* 25:1467–77

Yin R, Feng X, Wang J, Bao Z, Yu B, Chen J. 2013b. Mercury isotope variations between bioavailable mercury fractions and total mercury in mercury contaminated soil in Wanshan mercury mine, SW China. *Chem. Geol.* 336:80–86

Yin R, Feng X, Wang J, Li P, Liu J, et al. 2013c. Mercury speciation and mercury isotope fractionation during ore roasting process and their implication to source identification of downstream sediment in the Wanshan mercury mining area, SW China. *Chem. Geol.* 336:72–79

Zambardi T, Sonke JE, Toutain JP, Sortino F, Shinohara H. 2009. Mercury emissions and stable isotopic compositions at Vulcano Island (Italy). *Earth Planet. Sci. Lett.* 277:236–43

Zheng W, Hintelmann H. 2010. Isotope fractionation of mercury during its photochemical reduction by low-molecular-weight organic compounds. *J. Phys. Chem. A* 114:4246–53